# Optimization of an Active Twist Rotor Blade Planform for Improved Active Response and Forward Flight Performance

Martin K. Sekula
NASA Langley Research Center
Hampton, Virginia

Matthew L. Wilbur
U.S. Army Research Laboratory
Hampton, Virginia

## Abstract

A study was conducted to identify the optimum blade tip planform for a model-scale active twist rotor. The analysis identified blade tip design traits which simultaneously reduce rotor power of an unactuated rotor while leveraging aeromechanical couplings to tailor the active response of the blade. Optimizing the blade tip planform for minimum rotor power in forward flight provided a 5 percent improvement in performance compared to a rectangular blade tip, but reduced the vibration control authority of active twist actuation by 75 percent. Optimizing for maximum blade twist response increased the vibration control authority by 50 percent compared to the rectangular blade tip, with little effect on performance. Combined response and power optimization resulted in a blade tip design which provided similar vibration control authority to the rectangular blade tip, but with a 3.4 percent improvement in rotor performance in forward flight.

## Background

Active rotors have been studied as a potential solution to a diverse range of problems plaguing rotary-wing vehicles. Numerous analytical and experimental studies have provided encouraging results indicating that vibration, noise, performance, as well as other issues may be successfully addressed through the use of trailing edge flaps, gurney flaps, active twist, and other active control concepts [1-11]. Some of these studies have also exposed potential limitations of active concepts – the inability of current state-of-the-art actuators to meet the control requirements necessary to fully achieve the potential benefits [11]. Volumetric constraints and the challenges of operating in a rotating environment have led to a considerable effort being dedicated to maximizing actuator control authority through mechanical amplification and optimization of actuators, control surfaces, and structures [12-16].

The current approach to address the aforementioned control authority problem begins with viewing the problem from a different perspective. Instead of redesigning an actuator, control surface, etc., to improve its deflections or its application force to provide more control authority over a problem (vibration, noise, etc.), this study examines how a rotor blade tip can be designed to improve the blade response to an actuator input and thereby achieve the required control authority without more stringent actuator requirements. Previous work on active-twist rotor designs have examined the effect of various structural parameters on blade response and rotor power [17, 18]. Optimization of the blade structure and actuator positioning has also been performed [12, 13]. Finally, a limited, but more pertinent, parametric study examining the effect of blade tip sweep, taper, and anhedral on rotor vibration, performance, and response has been conducted previously [19]. The present work will expand on these results by performing an optimization study of a more complex blade tip planform than considered previously. While there have been multiple blade planform optimization studies conducted previously, they have examined the aerodynamic design in an effort to improve performance, reduce noise, reduce vibration, or some combination of these goals [20-23]. None have specifically dealt with active control improvements. The ultimate goal of this study is to develop a proof of concept for employing the blade tip design to improve the control authority of an active rotor – in this case study, an active twist rotor – and with this proof of concept identify limitations of the general approach and areas for further research and development.

## Blade Design

The baseline blade design used in this study is similar to that used in the aerodynamic design study of the Advanced Active Twist Rotor (ATR) [19]. This model-scale rotor has a radius of 4.685 feet and a hover tip Mach number of 0.628. The rotor is assumed to operate in a heavy gas environment used for testing at the Langley Transonic Dynamics Tunnel, which reduces the speed of sound by approximately 50 percent. For simplicity, the model assumes all structural axes and the aerodynamic center of the blade sections are located at the local quarter chord. The outer 10 percent of the blade is divided into five 0.02R segments where the blade chord and sweep angle can be varied independently within each segment. The sweep angle is assumed to be constant within each segment, while the chord length varies linearly within each segment. The

Presented at the Fifth Decennial AHS Aeromechanics Specialists' Conference, San Francisco, CA, January 22-24, 2014.

rate of taper within each segment is specified by defining the chord length at the outboard edge of the segment. The range of values for the design parameters examined in this study is presented in Table 1. The baseline blade planform, including the location of the blade tip segments, is presented in Figure 1.

The Advanced ATR study examined four blade design parameters: constant sweep, constant anhedral, and linear taper in the outer five percent of the blade and linear blade twist of the entire blade. The blade active twist response was found to be most sensitive to variations in sweep and taper [19], therefore the present study limited the tip design parameters to just sweep and chord length. While anhedral was found to also have a beneficial effect on twist response and on rotor power, for the purposes of this study it was deemed more important to reduce and simplify the design space and thereby keep the analysis of the final optimized designs more manageable.

To simplify the analysis, the elastic properties of the blade tip are assumed to be constant, and thereby insensitive to changes of the local chord or sweep. Within each blade tip segment, the structural axes are adjusted based on the local sweep angle, and the sectional mass of each segment is assumed to be a linear function of the local chord. For each design examined, a non-structural mass is added, if necessary, at 0.9R to constrain the overall blade chordwise-CG location to the blade pitch axis, which is coincident with the blade quarter-chord inboard of 0.9R. A single design constraint is imposed on the design space to help maintain the aeroelastic stability of the design – the aerodynamic center of the blade tip must be on or aft of the quarter chord of the inboard blade section.

*Analytical Rotor Model*

The aeroelastic behavior of the active twist rotor was modeled using the second generation version of the Comprehensive Analytical Model of Rotorcraft Aerodynamics and Dynamics (CAMRAD II) analysis software [24]. The finite element model of the rotor blades included flap, lag, and torsion degrees of freedom. The aerodynamic loads acting on this rotor were modeled with a 22-panel lifting line analysis, which employed C81 tables for lift, drag, and pitching moment coefficients. In forward flight at an advance ratio of 0.3, a free wake model was employed with a single tip trailer extending for five revolutions. For the response calculation, a uniform inflow model was employed. CAMRAD II does not have a direct capability for modeling the strain-induced actuation of a rotor blade due to embedded actuators, therefore, the active-twist actuation was modeled by imposing a torsional moment couple located at the ends of the active portion of the rotor blade, 0.2489R and 0.9R. A wind-tunnel trim approach was employed to trim the rotor to a lift coefficient, $C_L/\sigma$, of 0.0756, a rotor drag coefficient, $C_D/\sigma$, of 0.00591, and to eliminate the first-harmonic blade flapping with respect to the rotor shaft.

CAMRAD II's regulator loop was included in the analysis of select blade designs to minimize the 4/rev vertical hub force vibration by adjusting the sine and cosine components of a 4/rev active twist control input. Such an approach was analogous to a procedure used in wind tunnel testing of the original ATR: an initial trim solution is determined without active twist control, then a secondary post-trim analysis is conducted where the rotor controls are frozen and the regulator loop determines the active twist control setting to minimize the vibration.

Table 1. Range of values for blade tip parameters.

| Parameter | Range |
|---|---|
| Sweep | -10 deg to 30 deg |
| Taper | 0.2c to 1.2c |

## Objective Function

The design approach employed in the present study is based on previous observations that active twist can readily alleviate loads and vibration, but provides marginal benefits for rotor power reduction [7, 17]. Therefore, an objective function, defined below, was developed to identify blade tip designs that maximize the blade active-twist response while simultaneously minimizing unactuated rotor power.

$$J = w_1 \frac{J_{FRF}}{J_{FRF_{bl}}} + w_2 \left( \frac{2P_{bl} - P}{P_{bl}} \right)_{\mu=0.3}$$

Where $P$ is the total power at an advance ratio of 0.3,

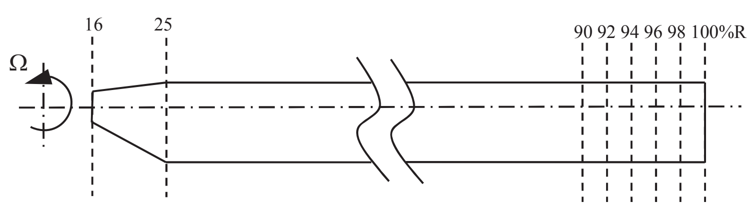


Figure 1. Baseline blade planform and tip design parameter locations.

$J_{FRF}$ is the frequency response objective function in hover (discussed below), $w_1$ and $w_2$ are weighting coefficients, and the subscript "*bl*" indicates values for the baseline design – a rectangular blade tip.

*Frequency Response Objective Function*

The active-twist frequency response function (FRF) is used to gauge the potential active-twist actuation effectiveness of an ATR design. A representative FRF and an ideal FRF, discussed below, are presented in Figure 2. Previous ATR design studies have relied on subjective judgment to ascertain the adequacy of the active-twist frequency response. In general, a good candidate design should have a large active-twist response at the frequencies of actuation ($N$-1, $N$, $N$+1/rev, where $N$ is the number of blades), since a larger response corresponds to a lower actuation voltage required to produce a specified level of active twist. At the same time, the FRF of an ideal design would exhibit a flat, unchanging response in the same frequency range ($N$-1/rev to $N$+1/rev), see Figure 2. This flat response is employed as a method to reduce active-twist sensitivity to modeling deficiencies and manufacturing inaccuracies and limitations. These and other uncertainties in the design and manufacturing process can change the magnitudes of peaks and troughs in the active-twist FRF or affect the frequencies at which they occur, potentially resulting in rotor blades with unexpected or underperforming active-twist control authority. Therefore, reducing the waviness, or undulations, of the active-twist FRF helps to produce a more robust design for an active-twist rotor.

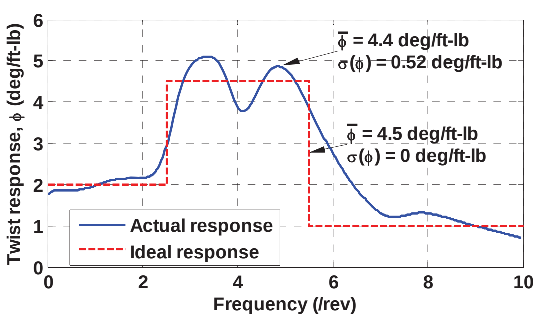


Figure 2. Ideal active twist frequency response function.

The characteristics of the active-twist FRF for candidate designs – the response magnitude and waviness – are quantified by determining the mean and standard deviation of the FRF within a frequency range of interest. For the current analysis, this range was set to 2.5/rev to 5.5/rev, presuming active vibration control for a 4-bladed rotor. Since waviness in the FRF is an undesirable trait, the standard deviation is employed as a penalty function. Based on this approach, the objective function, $J_{FRF}$, can be defined as

$$J_{FRF} = \bar{\phi} - w_{\sigma}\sigma(\phi)$$

where $\bar{\phi}$ is the average value of the FRF in the frequency range of 2.5/rev to 5.5/rev, $\sigma(\phi)$ is the standard deviation of the FRF across this frequency range, and $w_{\sigma}$ is the weight coefficient for the standard deviation function.

## Optimization Methodology

The optimization process utilized in this study consists of two steps where non-gradient and gradient-based optimizations are applied successively to determine an optimal design. A genetic algorithm (GA) was chosen for the initial, global optimization since the design space may be non-linear, raising the possibility that a gradient-based approach may converge to a local minima. The GA was coupled with a response surface (RS) metamodel of the design space to provide a computationally efficient approach to determine an approximate optimum design. This design is then used as a starting point by the gradient-based optimizer to identify the optimum design. Each of these steps, including the metamodel development, will be discussed in greater detail below.

*Non-Gradient-Based Optimization*

The non-gradient-based optimization algorithm employed in this analysis is the FORTRAN Genetic Algorithm Driver by David L. Carroll. It analyzed the RS metamodel to identify a preliminary optimal design. The GA uses 4000 generations with a population size of 50 designs. The jump mutation, creep mutation, and crossover probabilities are set at 2, 4, and 50 percent, respectively. Each pair of "parents" is allowed one "child" and elitism is enforced. Each degree of freedom of the design space is discretized into 5 equally spaced sweep angles or 6 equally spaced chord lengths across their respective degrees of freedom.

*Gradient-Based Optimization*

The gradient-based optimization employed in this analysis is the method of moving asymptotes (MMA). MMA was chosen due to its stability and speed of convergence characteristics [25]. The preliminary design identified by the GA analysis is used as the initial condition in the gradient-based optimization. Unlike the GA analysis, MMA does not employ a metamodel to approximate the design space, but at each step utilizes CAMRAD II solutions to determine the optimal design. This approach avoids the limitations of the metamodel or discretization of the design space required by the GA analysis.

*Response Surface Metamodel*

A response surface metamodel was employed in this analysis in order to improve the computational efficiency of the optimization process. It was decided that the computational cost reduction gained through the use of a metamodel outweighed the loss of design space fidelity. The metamodel of the design space consists of two response surfaces, one defining the active-twist response objective function, $J_{FRF}$, throughout the design space and another defining the cruise power, $P$. For simplicity, however, they will collectively be referred to as *the metamodel*.

The initial metamodel construction was based on CAMRAD II analyses of designs identified using a latin hypercube sampling. An iterative sampling approach is used to develop the metamodel. Initially, a random sampling based on the latin hypercube was used to develop a 10 variable, second-order metamodel. This initial metamodel was employed by the genetic algorithm optimization analysis to determine a best design. All the designs from the final generation of the GA were analyzed with CARMAD II and the results were employed to update the metamodel. Using the full generation, not just the best design, provided a level of randomness to the distribution of design sampling throughout the design space, yet simultaneously provided an emphasis on the region around the best design. This updating process was applied iteratively until the standard deviation between the metamodel and CAMRAD II-derived results converged to a minimum value. Every several iterations, the weight factors $w_1$ and $w_2$ were varied to remove any potential bias in the metamodel development towards higher fidelity of either the power or response metamodels of the design space.

Since the second order metamodel may not properly define the design space, a perturbation analysis was conducted by individually adding each of the 213 possible third-order terms to the metamodel in order to determine which terms reduced the metamodel error. The 3rd order terms to which the metamodel exhibited sensitivity were incorporated into the metamodel, and the iterative updating process was reinitiated to arrive at the final metamodel. This metamodel, used throughout the following study, is based on approximately 4000 designs.

## Results

*Impact of Standard Deviation Penalty Function*

An initial study was conducted to examine the impact of the weight coefficient of the standard deviation function, $w_\sigma$, on the shape of the active twist frequency response function. For each value of $w_\sigma$, the optimization process described above was conducted to determine a blade design which optimizes the blade response without any rotor power considerations ($w_2$ =0.) The effect of $w_\sigma$ on the active twist frequency response function is presented in Figure 3. The value of $w_\sigma$ was varied from 0 to 4 where larger values indicate more emphasis in the optimization process on reducing the variability of the FRF magnitude in the 2.5/rev to 5.5/rev range. Blade tip designs identified based on $w_\sigma$ values ranging from 0 to 2 do not produce a large change in the FRF. For these designs the value of $\sigma(\phi)$ in the 2.5/rev to 5.5/rev range is small compared to the mean value of the FRF in the same frequency range, and therefore $\sigma(\phi)$ had a limited influence on the final optimized design. When the weight factor $w_\sigma$ was increased to 3 or greater, the optimization process started to identify designs with smaller standard deviation values, but at a cost of a reduced mean FRF value. For the subsequent analyses conducted in this study, a $w_\sigma$ value of 3 was chosen based on the FRFs presented in Figure 3, since this $w_\sigma$ value produced a design exhibiting an FRF with a large mean and a more limited variability in the frequency range of interest.

*Effect of Objective Functions on Tip Design*

A series of design optimization studies was conducted to determine blade tip designs which are most effective at increasing active twist effectiveness, improving blade performance, or combining the benefits of both. Figure 4 presents the blade planforms determined by these studies. Weight factors employed during these studies, total rotor power, response objective function characteristics, and the design properties for each optimized blade tip design are provided in Tables 2 and 3. Likewise, the active-twist FRFs for the baseline and the four optimized designs are presented in Figure 5.

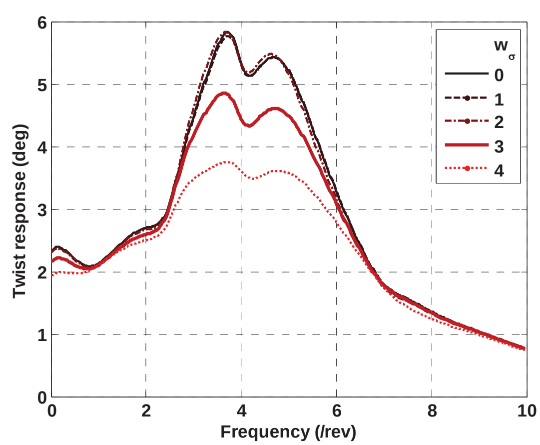


Figure 3. Sensitivity of active twist FRF to $w_\sigma$.

Table 2. Objective function weights, FRF characteristics, and total power.

| | $w_1$ | $w_2$ | $w_\sigma$ | $\bar{\phi}$ (deg/ft-lb) | $\sigma(\phi)$ (deg/ft-lb) | $P_{\mu=0.3}$ (hp) | $P_{\mu=0.3}$† (hp) |
|---|---|---|---|---|---|---|---|
| Baseline | - | - | - | 2.815 | 0.127 | 11.677 | 11.418 |
| Power | 0 | 1 | 0 | 1.774 | 0.187 | 11.073 | 10.772 |
| Response | 1 | 0 | 3 | 4.338 | 0.416 | 11.670 | 11.388 |
| Combined | 1 | 1 | 3 | 4.183 | 0.403 | 11.284 | 10.983 |
| Weighted | 0.5 | 1 | 3 | 3.873 | 0.384 | 11.210 | 10.955 |

†Multiple trailer wake model.

Table 3. Design parameter values.

| | Sweep (deg) | | | | | Chord ($c/c_{bl}$) | | | | |
|---|---|---|---|---|---|---|---|---|---|---|
| Segment | 1 | 2 | 3 | 4 | 5 | 1 | 2 | 3 | 4 | 5 |
| Baseline | 0.00 | 0.00 | 0.00 | 0.00 | 0.00 | 1.000 | 1.000 | 1.000 | 1.000 | 1.000 |
| Power | 30.00 | 30.00 | 30.00 | 30.00 | 30.00 | 0.718 | 0.673 | 0.565 | 0.352 | 0.206 |
| Response | -9.56 | -8.59 | 27.33 | 23.81 | 19.83 | 0.352 | 0.877 | 1.111 | 1.198 | 0.293 |
| Combined | -9.23 | -4.57 | 29.98 | 29.94 | 29.91 | 0.708 | 0.891 | 0.882 | 0.704 | 0.203 |
| Weighted | -9.53 | -0.42 | 30.00 | 29.96 | 29.94 | 0.666 | 0.927 | 0.623 | 0.562 | 0.203 |

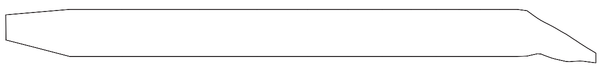

(a) Total power.

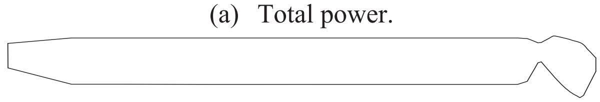

(b) Blade active-twist response.

(c) Combined power and blade active-twist response.

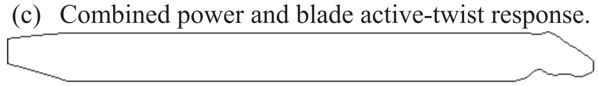

(d) Power-weighed combined design.

Figure 4. Optimized blade planforms.

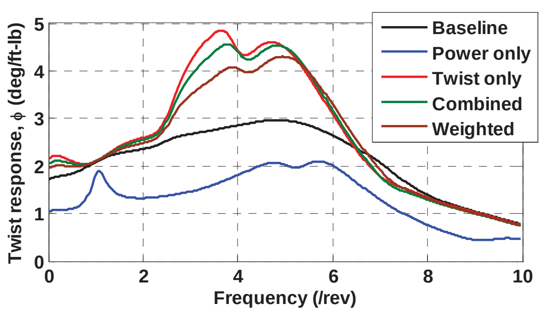


Figure 5. Active twist frequency response function at 0.9R.

The unactuated vibration magnitude at an advance ratio of 0.3, minimized vibration magnitude resulting from active twist actuation, and the corresponding active twist control magnitude are provided in Table 4. The information for a rectangular tip baseline design is provided for comparison in all tables and figures.

The power-only optimized design, Figure 4a, is a swept-tapered blade tip providing the best forward flight performance – a 5 percent reduction in power compared to the baseline (rectangular) tip design – but exhibiting the worst active-twist mean response, $\bar{\phi}$. A comparison of active twist FRFs for the power-optimized design and the baseline design reveals that in the 3/rev to 5/rev range the power-optimized design has a 30 to 50 percent lower response. The product of this limited twist response can be observed in Table 4, where the power-optimized rotor required the largest control magnitude to eliminate vibration, even though that rotor produced the least vibration during unactuated operation. In fact, the vibration control authority – vibration reduction per unit of active-twist actuation – is 25 percent of the baseline design control authority. While this design exhibits low unactuated vibratory loads, which implies that maybe active vibration control is not warranted for this design, it should be noted that this low response also affects other potential active twist applications such as noise or blade load reduction.

The active twist response-optimized tip planform is presented in Figure 4b and design parameters are provided in Table 3. This design has an unconventional tip geometry. The inner two blade tip segments sweep forward followed by an aft sweep for the outer three segments. This aft sweep is required to satisfy the design constraint placed on the aerodynamic center of the blade tip. The chord of the blade significantly narrows between 0.9R and 0.92R, the inner-most segment, followed by a steady increase in the chord between 0.92R and 0.98R, with a final taper to the blade tip. This tip design provided the largest response, approximately 50 percent higher than the baseline, but the rotor required the most power in forward flight of the optimized designs presented (see Table 2). It should be acknowledged that this design may not be feasible due to structural limitations that may arise from the small chord at 0.92R, making it impractical to build. Other design constraints would need to be added to

Table 4. Baseline vibration and actuated vibration and corresponding control magnitude at μ=0.3.

| | Baseline | Power | Response | Combined | Weighted |
|---|---|---|---|---|---|
| $F^{4P}_{z\ unactuated}$ (lbs) | 16.06 | 5.122 | 15.76 | 13.76 | 13.15 |
| $F^{4P}_{z\ actuated}$ (lbs) | 0.4098 | 0.3524 | 0.3153 | 0.3480 | 0.3527 |
| Actuation (ft-lbs) | 0.3280 | 0.4023 | 0.2142 | 0.2771 | 0.3546 |
| Control authority (lbs/ft-lbs) | 47.70 | 11.86 | 72.10 | 48.40 | 36.28 |

address these concerns. The unactuated vibratory loads at $\mu = 0.3$ are slightly lower than the baseline loads, but the amount of actuation required to almost completely eliminate the vibration is reduced significantly, resulting in a 50 percent increase in vibration control authority (see Table 4.) Like the baseline, this design has a vibration control authority that is significantly greater than the power-optimized design, but the large disparity in unactuated vibratory loads between this design and the power-optimized design suggests that vibratory loads should be included in the objective function used in the optimization process.

The blade tip designs determined by combined power and response optimization, Figures 4c and 4d, incorporate the characteristics of both the power-optimized and response-optimized designs. The first of these two composite designs, labeled "Combined," placed an equal emphasis on both power and response by employing equal values for weight factors $w_1$ and $w_2$ in the objective function, $J$. The planform, presented in Figure 4c, looks like an amalgamation of the response-optimized and power-optimized designs. This tip design provides a large response, close in magnitude to the response-optimized design (see Figure 5), while simultaneously requiring 3.4 percent less power in forward flight than the baseline design. The unactuated vibratory loads produced by this rotor design are approximately 15 percent lower than the baseline design loads, with a vibration control authority on par with the baseline design. Therefore, this tip design provides an improvement in power required without any significant degradation in active twist control authority.

The equal weighting between power and twist response resulted in a design with two percent higher rotor power than the power-optimized design, while exhibiting a minor degradation in the frequency response function (see Table 2 and Figure 5). Therefore, a second composite design was developed, labeled "Weighted," which placed more emphasis on minimizing rotor power by setting the values of weight factors $w_1$ and $w_2$ to 0.5 and 1.0, respectively. The resulting tip planform is similar to the "Combined" design (compare Figures 4c and 4d). It has a little less forward sweep, particularly in the second segment, and some minor differences in blade chord (compare Table 3). The power required at $\mu = 0.3$ is 4 percent lower than the baseline design – a 0.5 percent improvement over the "Combined" design. This improvement in performance came at a cost of reduced vibration control authority (see Table 4), indicating that detailed design studies should be conducted weighing the benefits of improved rotor performance versus improved active control.

The aerodynamic model employed throughout the optimization procedure was a single tip trailer free wake model. This low-fidelity aerodynamic model leaves to question the validity of the presented optimized designs. Previous studies have indicated that the wake model has a limited, attenuating effect on the active twist FRF [18]. The validity of the power calculation was examined by analyzing the final optimized designs in forward flight with a multiple-trailer free wake model. Computational considerations limited the number of trailers to 10, which were assigned to the outboardmost 9 aerodynamic panels. The updated rotor power is provided in Table 2. The single-trailer free wake model overpredicted the rotor power for all the rotor designs, but the trends remained the same.

The fan plots for the baseline rotor and the four optimized blade designs discussed above are presented in Figure 6. All fan plots were calculated in hover at a constant collective pitch of 8 degrees. The modal frequencies at the nominal rotational velocity and

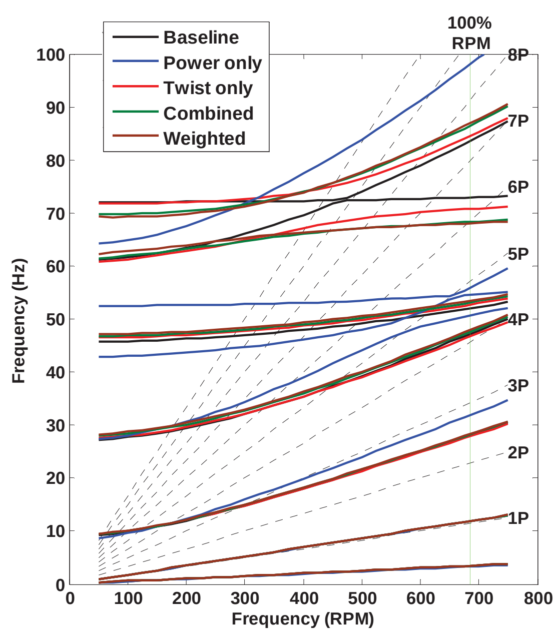

Figure 6. Fan plots for various blade designs.

Table 5. Blade mode frequency and identification

| Baseline | | Response | | Power | | Combined | | Weighted | | Power (no mass) | |
|---|---|---|---|---|---|---|---|---|---|---|---|
| Freq. | Mode | Freq. | Mode | Freq. | Mode | Freq. | Mode | Freq. | Mode | Freq. | Mode |
| 0.305 | L | 0.305 | L | 0.292 | L | 0.305 | L | 0.306 | L | 0.308 | L |
| 1.043 | F | 1.042 | F | 1.041 | F | 1.043 | F | 1.043 | F | 1.043 | F |
| 2.46 | F-L | 2.44 | F-L | 2.79 | F-L-T | 2.47 | F-L-T | 2.48 | F-L-T | 2.44 | F-L |
| 4.13 | F-L | 4.09 | F-L-T | 4.44 | T-F | 4.17 | F-L-T | 4.20 | F-L-T | 4.08 | F-T |
| 4.56 | L-F-T | 4.62 | L-F-T | 4.78 | T-F | 4.65 | L-F-T | 4.68 | L-F | 4.77 | L-F-T |
| 6.39 | T | 6.20 | T | 4.88 | F-T | 5.98 | T | 5.96 | T | 5.70 | T |
| 7.32 | F-L-T | 7.40 | F-T | 8.58 | F-T | 7.58 | F-T | 7.62 | F-T | 7.82 | F-T |

F= flap L = lag T=torsion

identification of each mode are provided in Table 5. The "combined" and "weighted" designs appear to have almost identical fan plots, and the response-optimized design frequencies do not vary significantly for the two composite designs until frequencies above 5/rev. It should be noted that the fourth elastic mode of these two designs –predominantly a torsion mode – falls very close to 6/rev, an undesirable design trait that can be avoided through the use of a design constraint on frequency placement [25]. This fourth elastic mode frequency placement of the response-optimized design is higher than that of the composite designs – closer in frequency to the baseline design – an indication that the large response of the two composite designs is not dependent on a resonant frequency.

The fan plot for the power-optimized rotor is significantly different from all the other designs. One of the most striking features of this fan plot is that the torsion mode frequencies are significantly lower than the other designs. This observation suggests that a torsionally stiffer design, or one with a lower torsional inertia, may be beneficial for designing an active twist rotor with a large active-twist response. Also of note is the fact that the frequencies of the first three elastic modes are higher than the other designs, and the frequencies of the remaining elastic modes also differ significantly from other designs, see Table 5. The structural properties of the inboard 90 percent of the blade are the same for all designs, and the blade tips vary only in their structural axes placement, which is sweep angle dependent, and in mass which has running mass and balance mass components.

The fan plots comparing the power-optimized design with and without a balance mass are presented in Figure 7 (the baseline rotor fan plot is provided for reference.) The balance mass in the power-optimized design accounts for 10 percent of the total blade mass, as shown in Table 6. Removing this balance mass has a significant influence on the frequency placement and mode shapes. The frequencies of four of the first five elastic modes reduce significantly, indicating that centrifugal stiffening produced by the balance mass has a dominant effect on the frequency placement. Modes that are dominated by torsional motion occur at higher frequencies.

The impact of the balance mass on the active-twist FRF is presented in Figure 8. The presence of the balance mass significantly attenuates the overall magnitude of the FRF. Without the balance mass, the power-optimized design has a response in the 2.5/rev to 5.5/rev range of similar magnitude to the response-optimized design, but with a significant amount of the undesirable

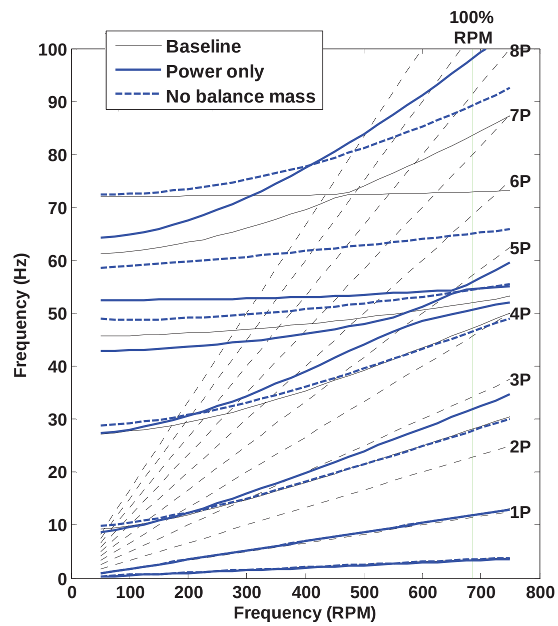


Figure 7. Power-optimized design fan plots with and without balance mass.

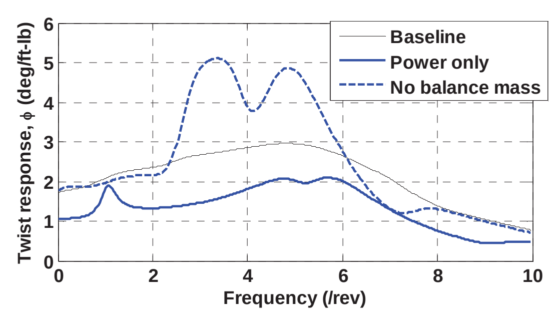


Figure 8. Frequency response function of power-optimized design with and without balance mass.

undulation not present in the FRF of the response-optimized design.

Table 6. Total blade mass and balance mass (slugs).

| | Blade | Balance Mass |
|---|---|---|
| Baseline | 0.1467 | - |
| Response | 0.1456 | 0.000002 |
| Power | 0.1607 | 0.0168 |
| Combined | 0.1462 | 0.00120 |
| Weighted | 0.1461 | 0.00164 |

*Perturbation analysis*

The design resulting from the combined response-power optimization, or "Combined" design, was employed as the basis for a perturbation study of each blade tip design variable. Each design variable was varied across its design range in 20 equal increments. For each design examined, the balance mass was adjusted to maintain the overall blade center of gravity on the pitch axis. The effect of varying the sweep and taper of each segment on the blade active-twist response at 0.9R is presented in Figure 9. The FRF of the optimum design is presented in green while the FRFs of the adjusted designs are color coded from red to blue, each color signifying the value of the adjusted design variable. The FRFs for the minimum and maximum values of the design variable are denoted by increased line thickness.

In general, active twist response of the blade is more sensitive to blade tip sweep variation than chord variation. The sweep variation of the inner two segments, Figures 9a and 9c, have the largest impact on amplitude of the FRF. Forward sweep in both segments increases the active twist response while the aft sweep diminishes the response. Another notable characteristic of the FRFs is that the effect of the sweep angle on the overall FRF magnitude becomes more pronounced as the aft sweep of this segment is reduced. The range of perturbation of the third segment, 0.94 to 0.96R, Figure 9e, was limited by response convergence problems most likely arising from susceptibility to divergence caused by the forward sweep, not numerical instabilities in the solution. Increasing the aft sweep initially increases the twist response but above 22 degrees of sweep, the response tends to drop. Varying the sweep of the outer two segments produces smaller changes to the active twist FRF, but the trend in the magnitude of the FRF is reversed compared to the inboard segments. Aft sweep increases the twist response of the blade while forward sweep diminishes it.

The FRF is virtually insensitive to chord variation at 0.92R and 0.96R, Figures 9b and 9f since the aerodynamic centers of these segments are close to the pitch and shear center axes of the blade. The largest change in response of the rotor blade due to changes in chord occurs at blade stations 0.94R, 0.98R, and 1.0R. The chord variation at 0.94R tends to affect the FRF in the 3/rev range while chord variation at 0.98R affects the FRF in the 5/rev range, see Figures 9(d and g). The largest impact on the active twist FRF is produced by chord variation at the tip, Figure 9i. Decreasing the tip chord increases the response of the blade – since reducing the chord length reduces the aerodynamic damping of the torsion and out-of-plane response. In the optimized blade tip design, the quarter chord locations at 0.94R, 0.98R, and 1.0R have the largest chord-wise offset from the blade pitch and structural axes, which affect the flap-torsion coupling of the blade modes. As with the sweep variation, for the outer two segments there is a reversal in the trend in how the FRFs are affected by changes in chord length, compare Figures 9b and 9d to Figures 9g and 9i.

Additional insight can be gained by examining the changes in mode shapes caused by the perturbation of the design parameters. For brevity, the effect of the sweep angle of the inboardmost blade tip segment, Segment 1, and the effect of chord length of the outboardmost blade tip segment, Segment 5, will be examined in detail. Some general observations will be made for the remaining design variables.

The effect of variation in the sweep angle of the inboard most segment (Segment 1) on the out-of-plane ($\beta$), in-plane ($\zeta$), and torsion ($\phi$) mode shape components of the first four elastic modes is presented in Figure 10. For brevity, these three mode shape components will be referred to as flap, lag, and torsion components, respectively. The mode shapes presented in Figure 10 correspond to the FRFs presented in Figure 9a. The same color scheme used in Figure 9 is employed to identify how the mode shapes vary with changing sweep angle. The title of each mode shape provides the optimized design frequency, plus the range of frequencies of the mode due to the variation in the design parameter. The mode shapes are normalized with respect to the blade tip out-of-plane deflection. For each mode shape, the ordinate of the in-plane and out-of-plane component plots are on the same scale, while the torsion plot is scaled independently since there is no equivalence of scales for nondimensionalized deflections in torsion and bending. These figures do not provide any information about the magnitude of each mode relative to others, but they do provide insight into the interaction of the in-plane, out-of-plane, and torsion components of the response within each mode.

Figure 10a presents the flap, lag, and torsion components of the mode shape for the first elastic mode. This mode was identified as being primarily a flap mode with some lag and torsion coupling. This figure indicates that increasing the aft sweep of Segment 1 tends to reduce the coupling of the torsion response with the flap and lag response. There also occurs a change in the frequency of the mode caused by the additional balance mass required to maintain the blade center of gravity on the pitch axis. This additional mass contributes to the centrifugal stiffening of the blade.

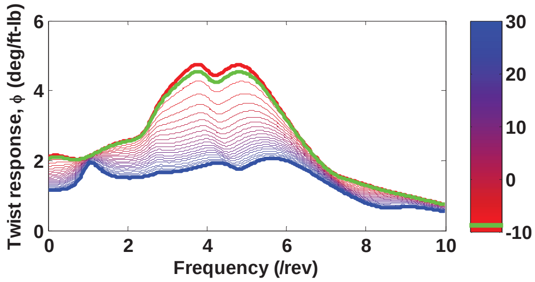


(a) Segment 1, sweep variation (0.90-0.92R)

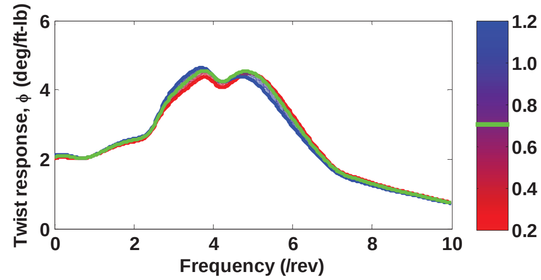


(b) Segment 1, chord variation (0.92R)

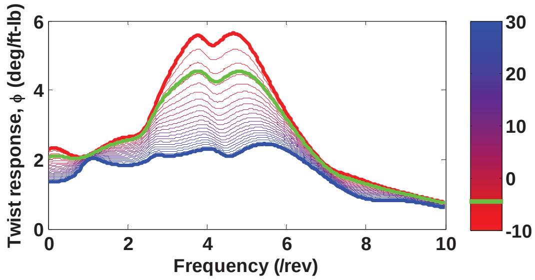


(c) Segment 2, sweep variation (0.92-0.94R)

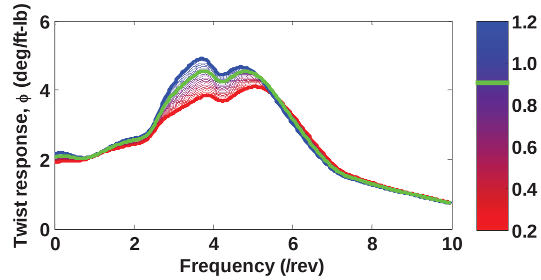


(d) Segment 2, chord variation (0.94R)

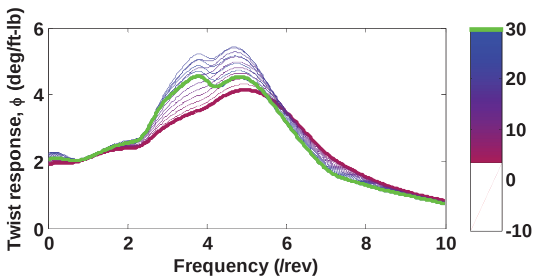


(e) Segment 3, sweep variation (0.94-0.96R)

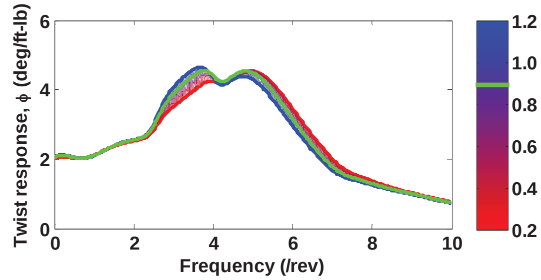


(f) Segment 3, chord variation (0.96R)

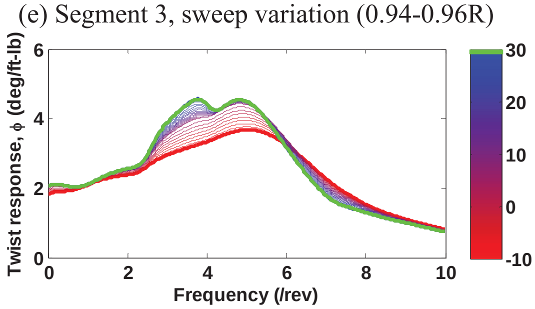


(f) Segment 4, sweep variation (0.96-0.98R)

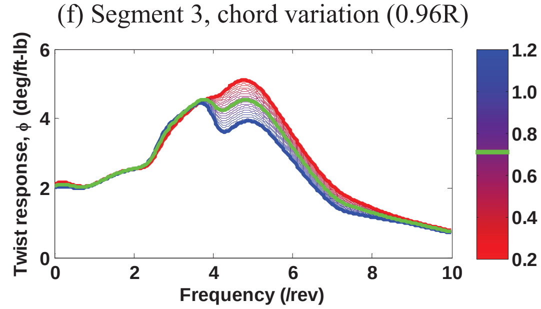


(g) Segment 4, chord variation (0.98R)

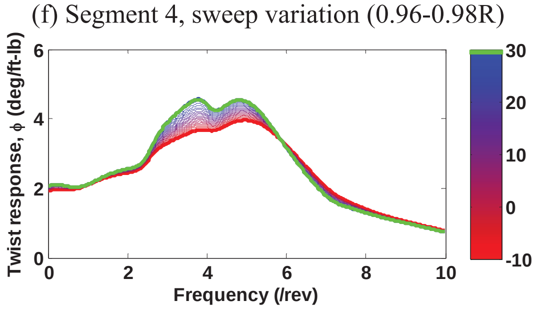


(h) Segment 5, sweep variation (0.98-1.0R)

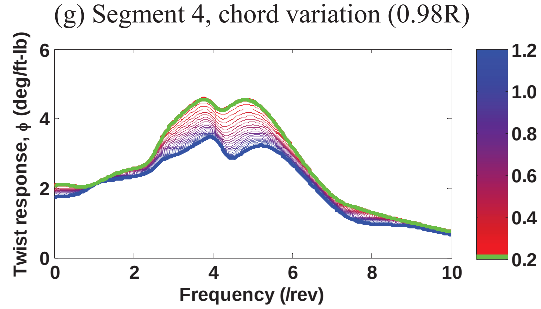


(i) Segment 5, chord variation (1.0R)

Figure 9. Effect of segment sweep and chord variation on twist frequency response function at 0.9R due to constant-amplitude active twist actuation (optimum design in green).

The effect of Segment 1 sweep variation on the second elastic mode (flap-lag-torsion) is presented in Figure 10b. Aft sweep increases the flap-torsion coupling while simultaneously increasing the lag component of the mode. The forward sweep of this segment in the optimized design results in a minimal coupling between the flap and torsion components of this mode. The lag component is also minimized.

The third elastic mode is presented in Figure 10c. Applying a more aft sweep in Segment 1 increases the flap-torsion coupling while reducing the lag component of this mode. Therefore, the forward sweep of the optimized design results in a coupled lag-flap response, with a very small torsion component.

The fourth elastic mode, Figure 10d, is a torsion mode with a limited flap component. Increasing the aft sweep increases the magnitude of the flap component relative to the torsion component. The frequency of this mode exhibits the most sensitivity to the sweep angle – the frequency drops from 6/rev to 4.9/rev as the sweep angle changes from -10 to 30 degrees.

The remaining four blade tip segments exhibited trends in mode shapes similar to those observed in Segment 1. The effectiveness of the sweep angle in Segment 2 increases since the aerodynamic center of this segment is ahead of the shear center and pitch axis of the blade. For the remaining outboard segments, the effectiveness of the sweep angle in adjusting the mode shapes and frequencies diminishes as the segment location approaches the blade tip. This reduction in effectiveness is more than likely due to the reduction in the area of the blade tip that is being moved in the chord-wise direction by the changing sweep angle.

The effect of chord length in Segment 5, the outer most blade tip segment, on the blade mode shapes is presented in Figure 11. The mode shape variation corresponds to the FRFs presented in Figure 9i. The ordinate range for the individual mode components match those used in Figure 10, thereby providing a means to assess the relative influence on the mode shapes of the sweep angle versus the chord length. Based on the changes in mode frequencies, the dominant effect of chord variation is observed on the second and fourth elastic flap modes. In both cases, the most sensitivity is observed in the torsion component of the modes. In the case of the second elastic flap mode, Figure 11b, decreasing the chord length of the segment reduces the flap-torsion coupling of the mode response. For the 4th elastic mode, predominantly a torsion mode, reducing the chord length causes a slight increase in the torsion response relative to the flap response, which results in a decrease in flap-torsion coupling (see Figure

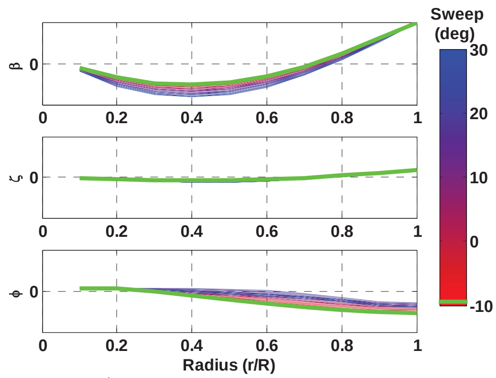


(a) 1st elastic mode 2.47P (2.47-2.80P)

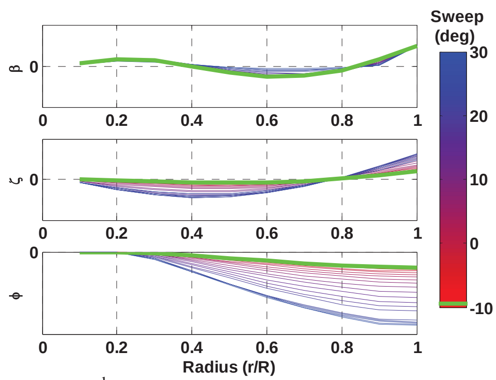


(b) 2nd elastic mode 4.17P (4.16 – 4.42P)

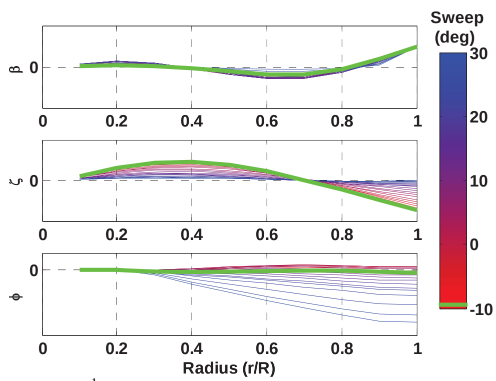


(c) 3rd elastic mode 4.65P (4.59P – 4.78P)

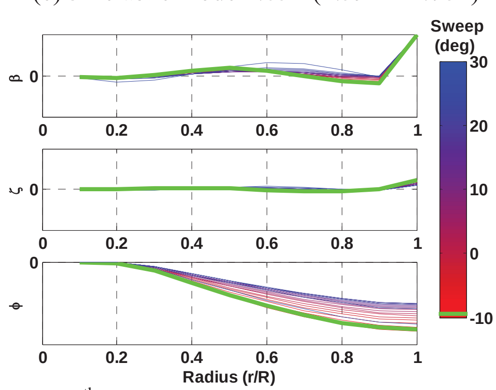


(d) 4th elastic mode 5.98P (4.91P – 6.02P)

Figure 10. Effect of sweep angle variation on blade mode shapes, Segment 1.

11d).  Similar observations can be made for the chord variation of the other segments in the blade tip.

## Conclusions

An optimization study was conducted to develop an advanced blade tip planform to maximize blade active twist control authority while simultaneously reducing forward flight rotor power requirements.  The design optimization was conducted in a two-step process using both gradient- and non-gradient-based optimization. First, a genetic algorithm coupled with a response surface metamodel was used to determine an approximate global optimum solution.  This solution was then the starting point in a gradient-based optimization which utilized a comprehensive analysis instead of a metamodel to determine the final design solution.  This approach was employed to develop blade tip designs optimized for either unactuated performance at an advance ratio of 0.3, active-twist response, or both.

The power-optimized blade tip design, a swept-tapered planform, reduced the power required by approximately five percent compared to a baseline, rectangular blade tip.  This design also produced the worst active-twist response, resulting in a 75 percent lower vibration control authority than the baseline design.  A large portion of this reduction in control authority is due to the large balance mass required by the aft sweep of the design.

A response-optimized blade tip design provided a 50 percent increase in active-twist response compared to the baseline design, while maintaining performance on-par with the baseline design.  This design had an unconventional planform which swept forward from 0.90 to 0.94R and then aft outboard of 0.94R, while the chord initially reduced at 0.92R then substantially increased until 0.98R, and then tapered towards the blade tip.

A combined power and response-optimized design, provided performance improvements of approximately 3.4 percent of baseline, with a minor degradation in the vibration control authority.  The blade planform was an amalgamation of the power-optimized and response-optimized designs.  Adjusting the weight factors in the objective function to emphasize performance resulted in minor changes in planform, with some gains in performance, but at a cost of a reduction in the vibration control authority.

Parametric studies of the individual design parameters about the combined power and response-optimized design indicated that forward sweep of the inboard section of the blade tip and the reduction in chord at the

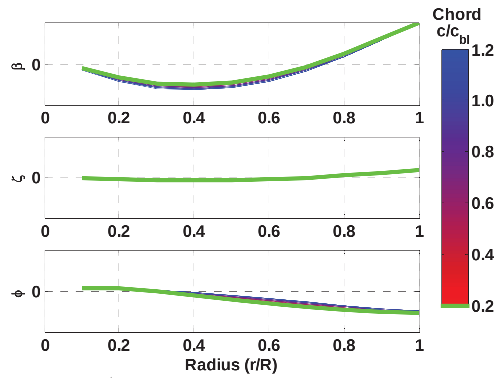


(a) 1st elastic mode 2.47P (2.47-2.59P)

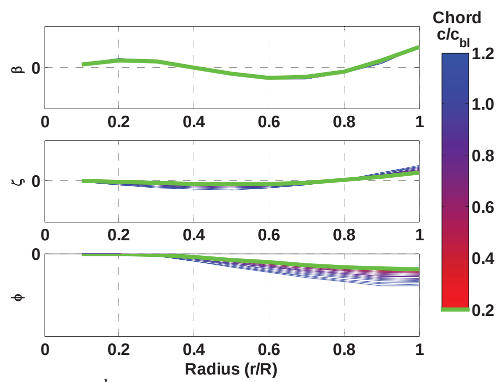


(b) 2nd elastic mode 4.17P (4.17 – 4.32P)

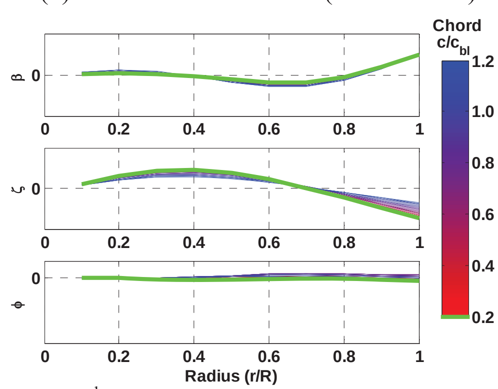


(c) 3rd elastic mode 4.65P (4.56P – 4.65P)

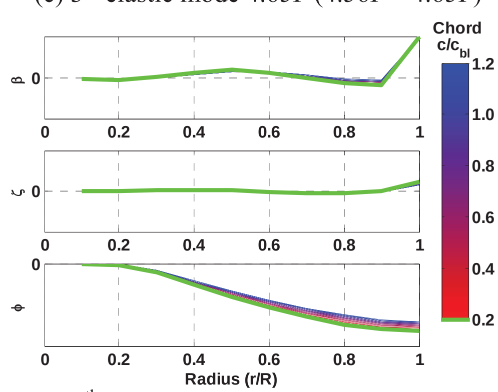


(d) 4th elastic mode 5.98P (5.46P – 5.99P)

Figure 11. Effect of chord length variation on blade mode shapes, Segment 5.

outboard sections of the blade tip provide the most improvement in active twist response. Analysis of mode shapes indicates that response-optimized blade tip designs tend to decouple the torsion response from flap and lag motion.

To further develop this concept, more modern optimization techniques and surrogate methods, such as multi-objective genetic algorithms and kriging interpolation, should be employed to identify optimum blade tip designs. Furthermore, design constraints addressing frequency placement and structural considerations should be implemented into the analysis. Higher fidelity aerodynamic and structural models should also be implemented to provide a higher confidence level in the optimized blade tip designs. Lastly, similar analyses should be performed on other active rotor concepts, such as active flaps, to determine what control authority benefits may be gained by tailoring the blade tip designs to a specific actuator.

## References


1. Baeder, J. D., Sim, B. W., "Blade-Vortex Interaction Noise Reduction by Active Trailing-Edge Flaps," Proceedings of the 54th Annual Forum of the American Helicopter Society, Washington, DC, May 1998.
2. Dawson, S., Straub, F., Booth, E., Marcolini, M., "Wind Tunnel Test of an Active Flap Rotor: BVI Noise and Vibration Reduction," Proceedings of the 51st Annual Forum of the American Helicopter Society, Fort Worth, TX, May 1995.
3. Depailler, G., Friedmann, P., "Alleviation of Dynamic Stall Induced Vibrations Using Actively Controlled Flaps," Proceedings of the 58th Annual Forum of the American Helicopter Society, Montreal, Canada, June 2002.
4. Min, B. Y., Sankar, L., Rojmohan, N., Prasad, J. V. R., "Computational Investigation of Gurney Flap Effects on Rotors in Forward Flight," *Journal of Aircraft*, Vo. 46, No.6, Nov.-Dec. 2009.
5. Brooks, T. F., Booth, E. R., Jr., "The Effects of Higher Harmonic Control on Blade-Vortex Interaction Noise and Vibration," *Journal of the American Helicopter Society*, Vol. 38 (3), July 1993.
6. Fogarty, D. E., Wilbur, M. L., Sekula, M. K., "A Computational Study of BVI Noise Reduction Using Active Twist Control," Proceedings of the 66th Annual Forum of the American Helicopter Society, Phoenix, AZ, May 11-13, 2010.
7. Wilbur, M. L., et al, "Vibratory Loads Reduction Testing of the NASA/Army/MIT Active Twist Rotor," Proceedings of the 57th Annual Forum of the American Helicopter Society, Washington, D. C., May 2001.
8. Gandhi, F., Sekula, M., "Helicopter Vibration Reduction using Fixed-System Auxiliary Moments," Proceedings of the 58th Annual Forum of the American Helicopter Society, Montreal, Canada, June 2002.
9. Kuefmann, P., Bartels, R., van der Wall, B., "On the Design and Development of a Multiple-Swashplate Control System for the Realization of Individual Blade Control (IBC) for Helicopters," Proceedings of the 67th Annual Forum of the American Helicopter Society, Virginia Beach, VA, May 2011.
10. Grohmann, B., et al, "Design, Evaluation and Test of Active Trailing Edge," Proceedings of the 67th Annual Forum of the American Helicopter Society, Virginia Beach, VA, May 2011.
11. Roget, B., Chopra, I., "Closed-Loop Test of a Rotor with Individually Controlled Trailing-Edge Flaps for Vibration Reduction," *Journal of the American Helicopter Society*, Vol. 55, No. 1, January 2010.
12. Thornburgh, R., Kreshock, A., Wilbur, M., "Structural Optimization of Active Twist Rotor Blades," Proceedings of the 67th Annual Forum of the American Helicopter Society, Virginia Beach, VA, May 2011.
13. Kumar, D., Cesnik, C., Rohl, P., Sutton, M., "Optimization Framework for the Dynamic Analysis and Design of Active Twist Rotors," Proceedings of the 68th Annual Forum of the American Helicopter Society, Fort Worth, TX, May 2012.
14. Zhang, J., Smith, E., Wang, K., "Active Passive Hybrid Optimization of Rotor Blades with Trailing Edge Flaps," *Journal of the American Helicopter Society*, Vol 49 (1), Jan. 2004.
15. Hall, S., Tzianetopoulou, T., Straub, F., Ngo, H., "Design and testing of a double X-frame piezoelectric actuator", Proc. SPIE 3985, Smart Structures and Materials 2000: Smart Structures and Integrated Systems, 26, June 22, 2000.
16. Ahci, E., Pfaller, R., "Structural Design, Optimization and Validation of the Integrated Active Trailing Edge for a Helicopter Rotor Blade," Proceedings of the 64th Annual Forum of the American Helicopter Society, Montreal, Canada, April 2008.
17. Sekula, M. K., Wilbur, M. L., Yeager, W. T., Jr., "A Parametric Study of the Structural Design for an Advanced Active Twist Rotor," Proceedings of the 61st Annual Forum of the American Helicopter Society, Grapevine, TX, June 1-3, 2005.
18. Wilbur, M. L., Sekula, M. K., "The Effect of Tip Geometry on Active-Twist Rotor Response," Proceedings of the 61st Annual Forum of the

American Helicopter Society, Grapevine, TX, June 1-3, 2005.

19. Sekula, M. K., Wilbur, M. L., Yeager, W. T., Jr., "Aerodynamic Design Study of an Advanced Active Twist Rotor," Proceedings of the American Helicopter Society 4th Decennial Specialist's Conference on Aeromechanics, San Francisco, California, January 21-23, 2004.
20. Yang, C., et al, "Blade Planform Optimization to Reduce HSI Noise of Helicopter in Hover," Proceedings of the 64th American Helicopter Society Forum, Montreal, Canada, April 2008.
21. Imiela, M., "High-Fidelity Optimization Framework for Helicopter Rotors," Proceedings of the 65th American Helicopter Society Forum, Pheonix, AZ, May, 2010.
22. Dumont, A., Le Pape, A., Peter, J., Huberson, S., "Aerodynamic Shape Optimization of Hovering Rotors Using a Discrete Adjoint of the Reynolds-Averaged Navier–Stokes Equations," *Journal of the American Helicopter Society*, **56**, 032002 (2011)
23. Collins, K., Sankar, L., Mavris, D., "Application of Low- and High-Fidelity Simulation Tools to Helicopter Rotor Blade Optimization," *Journal of the American Helicopter Society*, **58**, 042003 (2013)
24. Johnson, W., *CAMRAD II, Comprehensive Analytical Model of Rotorcraft Aerodynamics and Dynamics*, Johnson Aeronautics, Palo Alto, California, 1994.
25. Svanberg, K., "The Method of Moving Asymptotes – A New Method for Structural Optimization," *International Journal for Numerical Methods in Engineering*, vol. 24,1987, pp 359-373.
26. Glaz, B., Friedmann, P., Liu, L., "Helicopter Vibration Reduction Throughout the Entire, Flight Envelope Using Surrogate Based Optimization," Proceedings of the 63rd American Helicopter Society Forum, Virginia Beach, VA, May 2007.